

Motion of the charged test particle in the spinning nonlinear electromagnetic black hole

Nora Breton^{1,*}, Gustavo Gutierrez-Cano^{2,†} and Alberto A. Garcia-Diaz^{1,‡}

¹*Departamento de Física, Centro de Investigación y de Estudios Avanzados del I.P.N.,
Apdo. Postal 14-740, México City, Mexico*

²*Departamento de Física, División de Ciencias e Ingenierías, Campus León,
Universidad de Guanajuato, C.P. 37150, Leon, Mexico*



(Received 25 May 2022; accepted 14 July 2022; published 29 July 2022)

In this paper the motion of charged and uncharged test particles in the rotating nonlinearly charged black hole (BH) is examined. Its asymptotics can be de Sitter or anti-de Sitter, depending on the value of the nonlinear parameter; consequently this BH can present one, two or three horizons, the third one being the cosmological horizon in the de Sitter case. Angular and radial test particle motions are analyzed and compared with its linear electromagnetic counterpart, the Kerr-Newman black hole (KN-BH). Several differences arise with the KN-BH, namely, the equatorial asymmetry is enhanced by the nonlinear electrodynamic field and for charged particles the access to one of the poles is forbidden; besides, a second circular orbit in the neighborhood of the external horizon appears, and the presence of the nonlinear electromagnetic field increases the curvature producing bounded orbits closer to the horizon.

DOI: [10.1103/PhysRevD.106.024056](https://doi.org/10.1103/PhysRevD.106.024056)

I. INTRODUCTION

The recent improvement in astrophysical observations as well as the direct gravitational wave detection by LIGO [1], Advanced LIGO and Advanced Virgo [2] has led to the assembly of catalogs of black holes that have stimulated the study of test particle motion in the neighborhood of compact objects. Astrophysical compact objects are rotating and therefore in the context of the Einstein exact solutions there is a great interest in stationary solutions since, within some approximation, they resemble astrophysical black holes (BHs) or compact objects.

Moreover, some compact objects can possess strong magnetic fields in their vicinity and these fields can be described by nonlinear electrodynamics (NLE). Recently was presented, for static spherically symmetric metrics the general exact solution of Einstein equations coupled to NLE [3], with an arbitrary structural metric function, which, via a pair of independent Einstein equations, allows one to derive the single associated field tensor component \mathcal{E} , and the Lagrangian-Hamiltonian field function $\mathcal{L}\mathcal{H}$, which determines the entire solution, should it be singular or regular. Also, a number of Einstein-NLE static solutions have been derived so far, both singular and regular; however the challenge of determining a NLE stationary solution has been elusive. This was accomplished recently

and a stationary solution of the coupled Einstein-NLE equations was presented in Refs. [4,5]. These first exact solutions describe a rotating black hole endowed with mass, angular momentum, an electromagnetic nonlinear parameter and cosmological constant; they fulfill a set of four generalized “Maxwell equations” for the electrodynamic fields $F_{\mu\nu}$ and $P_{\mu\nu}$ and two independent Einstein-NLE equations related with the two independent eigenvalues of the NLE energy-momentum tensor. The NLE is determined by a Lagrangian function $L(F, G)$ constructed from the two electromagnetic invariants F and G .

We do not claim that these solutions represent in a feasible way real astrophysical objects, but neutron stars and gravastars are characterized by generating strong magnetic fields, then these kind of exact solutions of the Einstein-NLE equations can give insight in the search of interesting properties of BHs as well as can be useful as test beds of BH numerical simulations.

In this paper, we examine the rotating axisymmetric solution of the Einstein equations coupled with NLE that was recently presented in Ref. [4] and with a cosmological constant in Ref. [5]. This solution is characterized by five physical parameters, namely, the gravitational mass m , electric and magnetic charges f_1, g_1 (comprised in F_0), the NLE parameter β and the angular momentum a . The existence of horizons allows a BH interpretation; however the solution is not asymptotically flat due to the NLE field that renders a de Sitter or anti-de Sitter (AdS) asymptotics. The solution has the Kerr-Newman limit when the NLE parameter vanishes, $\beta = 0$, with the Kerr-Newman (KN)

*nora@fis.cinvestav.mx

†ggutierrezcano@ugto.mx

‡aagarcia@fis.cinvestav.mx

electric charge being $Q_e^2 = F_0$. For charged test particles the angular and radial motions are analyzed and compared with its linear electromagnetic counterpart, the Kerr-Newman black hole (KN-BH). Several differences arise in the motion of charged test particles, namely, the equatorial symmetry is not preserved and the access to one of the poles is forbidden and a second circular orbit can appear in the neighborhood of the external horizon; the allowed regions for the bounded test particle motion are illustrated in a series of plots varying the parameters of the system.

The paper is organized as follows. In the next section a brief review of NLE is presented. In Sec. III the stationary NLE BH is introduced and its horizons are analyzed. In Sec. IV the motion equations are derived; for charged and uncharged test particles, we analyze trajectories in both, θ motion and r motion. Some comments on birefringence are presented in Sec. V and final remarks are given in Sec. VI.

II. NONLINEAR ELECTRODYNAMICS

For completeness, we include the basic features of NLE. This theory is constructed from a Lagrangian function $L = L(F, G)$ that depends on the electromagnetic invariant F and pseudoscalar G

$$F = \frac{1}{4} F_{\mu\nu} F^{\mu\nu}, \quad G = \frac{1}{4} {}^*F_{\mu\nu} F^{\mu\nu}, \quad (1)$$

where the dual field tensor ${}^*F_{\mu\nu}$ is defined by

$${}^*F_{\mu\nu} := \frac{1}{2} \sqrt{-g} \epsilon_{\mu\nu\alpha\beta} F^{\alpha\beta}, \quad {}^*F^{\alpha\beta} = -\frac{1}{2\sqrt{-g}} \epsilon^{\alpha\beta\mu\nu} F_{\mu\nu}. \quad (2)$$

For coupled NLE with Einstein equations the corresponding energy-momentum tensor $T^{\mu\nu}$ can be derived from the variation of the matter Lagrangian L_M with respect to $g_{\mu\nu}$. In NLE one uses for the Maxwell limit the Lagrangian function $L_{\text{Max}}(\text{NLE}; F) = F^{\alpha\beta} F_{\alpha\beta}/4$, instead of the standard Maxwell Lagrangian function $L_{\text{Max}}(F) = -F$; thus, to obtain the Maxwell limit, one has to use the Lagrangian function $L_M = -L(\text{NLE}; F, G)$. Therefore, accomplishing the variations, one arrives at

$$\begin{aligned} -T^{\mu\nu} &= L g^{\mu\nu} - L_F F^{\mu\sigma} F^\nu{}_\sigma - L_G F^{\mu\sigma} {}^*F^\nu{}_\sigma \\ &=: L g^{\mu\nu} - F^{\mu\sigma} P^\nu{}_\sigma, \end{aligned} \quad (3)$$

where we have introduced the new field tensor $P_{\mu\nu}$, which one identifies as the $P_{\mu\nu}$ field tensor of Plebański [6], or the p^{kl} -field tensor of Born-Infeld [7]. $F_{\mu\nu}$ and $P_{\mu\nu}$ are related to each other by

$$\begin{aligned} P_{\mu\nu} &= 2 \frac{\partial L}{\partial F^{\mu\nu}} = L_F F_{\mu\nu} + L_G {}^*F_{\mu\nu}, \\ F_{\mu\nu} &= 2 \frac{\partial H}{\partial P^{\mu\nu}} = H_P P_{\mu\nu} + H_Q {}^*P_{\mu\nu}. \end{aligned} \quad (4)$$

To the antisymmetric field $P_{\mu\nu}$ there are associated its dual field tensor ${}^*P_{\mu\nu}$ and the invariants P and Q ,

$$\begin{aligned} {}^*P_{\mu\nu} &:= \frac{1}{2} \sqrt{-g} \epsilon_{\mu\nu\alpha\beta} P^{\alpha\beta}, \quad {}^*P^{\alpha\beta} = -\frac{1}{2\sqrt{-g}} \epsilon^{\alpha\beta\mu\nu} P_{\mu\nu}, \\ P &= \frac{1}{4} P_{\mu\nu} P^{\mu\nu}, \quad Q = \frac{1}{4} {}^*P_{\mu\nu} P^{\mu\nu}. \end{aligned} \quad (5)$$

The structure function $H(P, Q)$, associated with the Lagrangian function $L(F, G)$, can be determined by a Legendre transformation

$$L(F, G) = \frac{1}{2} F_{\mu\nu} P^{\mu\nu} - H(P, Q). \quad (6)$$

The electrodynamics is determined through the ‘‘Faraday-Maxwell’’ electromagnetic field equations, which in vacuum are

$$\begin{aligned} {}^*F^{\mu\nu}{}_{;\nu} &= 0 \rightarrow (\sqrt{-g} {}^*F^{\mu\nu})_{;\nu} = 0, \\ P^{\mu\nu}{}_{;\nu} &= 0 \rightarrow [\sqrt{-g} L_F F^{\mu\nu} + \sqrt{-g} L_G {}^*F^{\mu\nu}]_{;\nu} = 0, \end{aligned} \quad (7)$$

which can be written by means of a closed 2-form $d\omega = 0$,

$$\omega = \frac{1}{2} (F_{\mu\nu} + {}^*P_{\mu\nu}) dx^\mu \wedge dx^\nu = \frac{1}{2} (F_{ab} + {}^*P_{ab}) e^a \wedge e^b,$$

since $F_{\mu\nu}$ and ${}^*P_{\mu\nu}$ are curls.

In nonlinear electrodynamics, the energy-momentum tensor $T^\mu{}_\nu$, Eq. (3), allows for two different pairs of eigenvalues $\{\lambda, \lambda', \Lambda', \Lambda'\}$. One can show that a similar property, i.e., two pairs of different eigenvalues, is shared by the field tensors $F_{\mu\nu}$ and $P_{\mu\nu}$, although their eigenvalues are different. Moreover, the NLE $T^\mu{}_\nu$ possesses a nonzero trace

$$-T := -T^\mu{}_\mu = 4(L - L_F F - L_G G). \quad (8)$$

On the other hand, taking into account the relation $F^{\mu\sigma} {}^*F_{\nu\sigma} = G \delta^\mu{}_\nu$, one determines the traceless NLE energy-momentum tensor $\Upsilon_{\mu\nu}$ to be

$$\Upsilon^\mu{}_\nu := T^\mu{}_\nu - \frac{T}{4} \delta^\mu{}_\nu = L_F (F^{\mu\sigma} F_{\nu\sigma} - F \delta^\mu{}_\nu). \quad (9)$$

The rotating NLE BH is an exact solution of Eq. (7) coupled with Einstein equations, $G_{\mu\nu} = \kappa T_{\mu\nu}$, and we present the line element in the next section.

III. THE STATIONARY NLE BH

The NLE BH reported in Ref. [4] is a stationary axisymmetric solution of the Einstein equations coupled with NLE, characterized by five physical parameters, namely, the gravitational mass m , electric and magnetic charges f_1, g_1 (comprised in F_0), the NLE parameter β and the angular momentum a ; the Kerr-like line element is given by

$$ds^2 = \rho^2 d\theta^2 + \frac{a^2 \sin^2 \theta}{\rho^2} \left[dt - \frac{r^2 + a^2}{a} d\phi \right]^2 + \frac{\rho^2}{Q(r)} dr^2 - \frac{Q(r)}{\rho^2} [dt - a \sin^2 \theta d\phi]^2, \quad (10)$$

$$\rho^2 = r^2 + a^2 \cos^2 \theta, \quad (11)$$

$$Q(r) = \frac{\kappa F_0}{2} (1 - \beta r^2)^2 - 2mr + r^2 + a^2. \quad (12)$$

See Ref. [4] for details on the derivation of this solution.

The contravariant metric components that will be used in the Hamilton-Jacobi equation of the test particle are

$$g^{tt} = -\frac{1}{\rho^2 Q(r)} [(r^2 + a^2)^2 - a^2 \sin^2 \theta Q(r)], \quad (13)$$

$$g^{rr} = \frac{Q(r)}{\rho^2}, \quad (14)$$

$$g^{\theta\theta} = \frac{1}{\rho^2}, \quad (15)$$

$$g^{\phi\phi} = \frac{Q(r) - a^2 \sin^2 \theta}{Q(r) \rho^2 \sin^2 \theta}, \quad (16)$$

$$g^{t\phi} = \frac{a}{\rho^2 Q(r)} [Q(r) - (r^2 + a^2)]. \quad (17)$$

A. Horizons

The horizons are given by the roots of the polynomial $Q(r) = 0$, i.e., by the real positive solutions of

$$\frac{\kappa F_0 \beta^2}{2} r^4 + (1 - \kappa F_0 \beta) r^2 - 2mr + \frac{\kappa F_0}{2} + a^2 = 0. \quad (18)$$

In general there may be four roots [8] depending on the value of β and the sign of the parameter F_0 , which also defines the asymptotics of the solution (see Fig. 1). We analyze the two cases of F_0 being positive or negative.

- (1) Case $F_0 > 0$. In this case the asymptotic behavior is anti-de Sitter, and the electromagnetic field mimics a cosmological constant given by

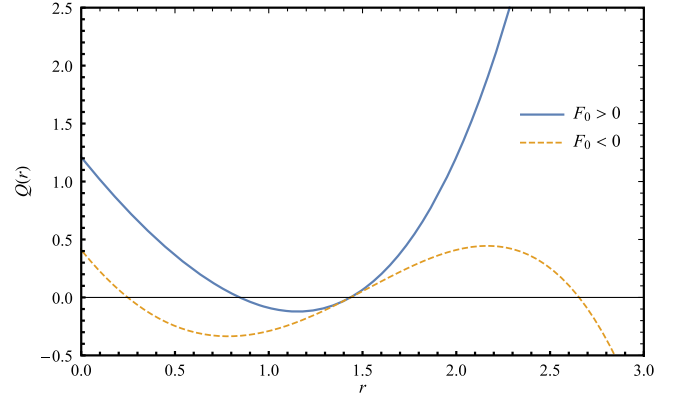


FIG. 1. The two possible asymptotics of the stationary NLE BH are shown; depending on the sign of F_0 the asymptotics of the solution is different. For $F_0 > 0$ there are inner and outer (event) horizons and the asymptotics is AdS, while for $F_0 < 0$ the solution presents three horizons—inner, outer and cosmological—and the asymptotics is de Sitter. In these plots the fixed parameters are $m = 1$, $\beta = 0.5$, $a = 0.9$ and $F_0 = \pm 0.8$.

$$\Lambda = -\frac{3}{2} \kappa F_0 \beta^2. \quad (19)$$

There are two values of r , $r_{1,2}^{\text{crit}}$ and two of β , $\beta_{1,2}^{\text{crit}}$, for which there is only one real root of $Q(r)$. These values are determined from $Q(r^{\text{crit}}, \beta^{\text{crit}}) = 0$ and $\partial_r Q(r^{\text{crit}}, \beta^{\text{crit}}) = 0$:

$$\begin{aligned} \frac{\kappa F_0 \beta^2}{2} r^4 + (1 - \kappa F_0 \beta) r^2 - 2mr + \frac{\kappa F_0}{2} + a^2 &= 0, \\ 2\kappa F_0 \beta^2 r^3 + 2(1 - \kappa F_0 \beta) r - 2m &= 0. \end{aligned} \quad (20)$$

From the second expression the values of β can be obtained

$$\beta_{1,2} = \frac{\kappa F_0 \pm \sqrt{\kappa F_0 [4(m-r)r + \kappa F_0]}}{2\kappa r^2 F_0}. \quad (21)$$

Substituting these values into the first expression, we arrive at a quadratic equation for r which can be solved using the Cardano-Ferrari method. For the different values obtained from β , the following cases occur:

- (a) $\beta < \beta_1^{\text{crit}}$. There are no real roots.
- (b) $\beta = \beta_1^{\text{crit}}$. A degenerate real positive root.
- (c) $\beta_1^{\text{crit}} < \beta < \beta_2^{\text{crit}}$. Two real positive roots.
- (d) $\beta = \beta_2^{\text{crit}}$. A degenerate real positive root.
- (e) $\beta > \beta_2^{\text{crit}}$. There are no real roots.

Examples of all these cases are illustrated in Fig. 2. The corresponding Carter-Penrose diagram of the black hole spacetime (two horizons) is shown in Fig. 3.

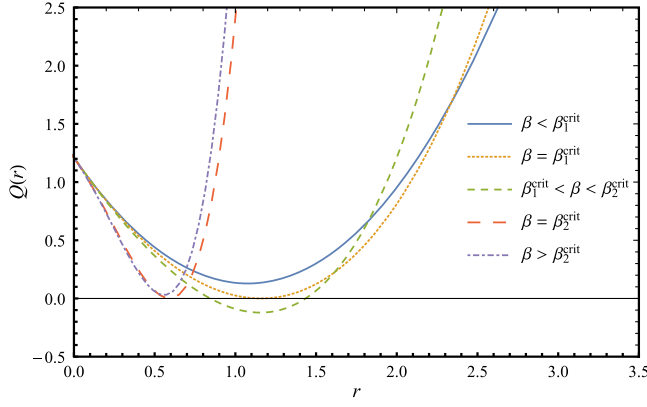


FIG. 2. The horizons for different values of β are shown. For $\beta < \beta_1^{\text{crit}}$ ($\beta > \beta_2^{\text{crit}}$) there are no horizons. For $\beta = \beta_1^{\text{crit}}$ ($\beta = \beta_2^{\text{crit}}$) there is a single degenerate double root, which corresponds to the extreme case with one horizon at $r_1^{\text{crit}} \approx 1.15$ ($r_2^{\text{crit}} \approx 0.59$). For $\beta_1^{\text{crit}} < \beta < \beta_2^{\text{crit}}$ there are two horizons. In this plot, we fix the parameters as $m = 1$, $a = 0.9$, $F_0 = 0.8$, $\beta_1^{\text{crit}} \approx 0.26$, and $\beta_2^{\text{crit}} \approx 3.54$.

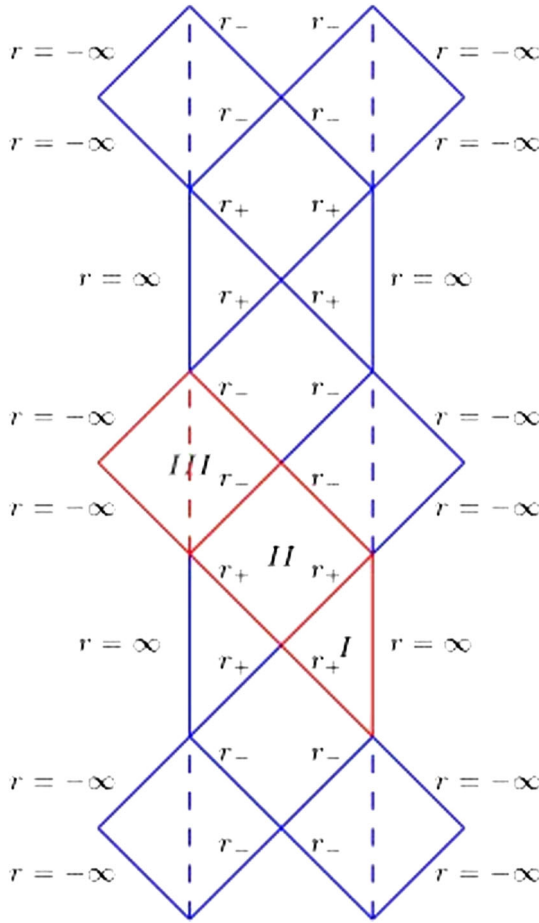


FIG. 3. The Penrose-Carter diagram of the rotating black hole with nonlinear electrodynamics. The dashed lines represent the ring singularity similarly to the Kerr-Newman BH.

- (2) Case $F_0 < 0$. In this case the asymptotic behavior is de Sitter, and the electromagnetic field acting as a cosmological constant is given by

$$\Lambda = -\frac{3}{2}\kappa F_0 \beta^2. \quad (22)$$

There are three positive real roots that represent an inner horizon, an outer horizon (event horizon), and a cosmological horizon, cf. Fig. 1.

In Figs. 1 and 2 the generic behavior of $Q(r)$ is shown. Note that at the origin, $Q(r=0)$, the metric function is finite; however, and this cannot be illustrated in a one-dimensional plot, the ring singularity, characteristic of the KN metric, persists in the stationary NLE-BH and occurs when simultaneously $r=0$ and $\theta = \pi/2$, i.e., when $\rho^2 = r^2 + a^2 \cos^2 \theta = 0$.

B. The ring singularity

In Ref. [9], it is analyzed the rotating Kerr-like spacetime and the conditions for the regularity of their second order polynomial invariants in the Riemann tensor. It was shown that the regularity of a Petrov type D spacetime coupled to a non-null electromagnetic field is determined by the finiteness of three invariant functions, namely the eigenvalue of the Weyl conformal tensor, the eigenvalue of the traceless Ricci tensor and the curvature scalar, $[\Psi_2, S, R]$ [10]. These invariants, for the Petrov type D solutions, are related to the Kretschmann quadratic Riemannian invariant by

$$\mathcal{K} = R_{\mu\nu\rho\sigma}R^{\mu\nu\rho\sigma} = 48\Psi_2\Psi_2^* + 8S^2 + \frac{1}{6}R^2. \quad (23)$$

For the metric (10) these invariants $[\Psi_2, S, R]$ are given by

$$\begin{aligned} 12\rho^6\Psi_2 &= (a \cos \theta - ir)^2 \{-12m(r + ia \cos \theta) \\ &\quad + 6\kappa F_0(1 - \beta^2 r^2 a^2 \cos^2 \theta) \\ &\quad + \kappa F_0 \beta [2(a^2 \cos^2 \theta - r^2) - 8ira \cos \theta]\}, \\ 2\rho^4 S &= \kappa F_0(1 + \beta[-a^2 \cos^2 \theta(1 - 3\beta r^2) + r^2]), \\ \rho^2 R &= 2\kappa F_0 \beta(1 - 3\beta r^2). \end{aligned} \quad (24)$$

Substituting these into Eq. (23), we obtain explicitly the Kretschmann invariant,

$$\begin{aligned} \mathcal{K} &= 48\frac{m^2}{\rho^6} - 48\frac{Q_e^2 m r}{\rho^8} + 14\frac{Q_e^4}{\rho^8} \\ &\quad + 16\frac{Q_e^2 \beta m r}{\rho^8} [-3x^2(1 - \beta r^2) + r^2] \\ &\quad + \frac{4Q_e^4 \beta}{\rho^8} [(x^2 - r^2) + \beta(r^4 + x^4 + r^2 x^2)] \\ &\quad + \frac{2\beta^3 Q_e^4 r^2}{\rho^8} [3\beta r^2(r^4 + 2r^2 x^2 + 6x^4) \\ &\quad - 2(r^4 - 3r^2 x^2 + 6x^4)], \end{aligned} \quad (25)$$

where we have taken $\kappa F_0 = Q_e^2$ as the BH electric charge and $x = a \cos \theta$. From the expression for the Kretschmann invariant, we see how the introduction of the NLE field affects the curvature. Assuming $\beta > 0$ the curvature is larger than that of KN, which corresponds to the first three terms. Accordingly, we shall see that for the rotating NLE BH the bounded orbits are closer to the horizon than for KN.

Moreover, the divergence of the Kretschmann invariant points to a real physical singularity at $\rho = 0$. We see from the previous expression that the divergence of the Stationary NLE BH is of the same order as in KN, $\mathcal{K} \approx \rho^{-8}$ and the inclusion of the NLE field into the Kerr-like metric does not introduce any singularity, apart from the characteristic ring singularity of the Kerr family, at $\rho = 0$, where the curvature invariant \mathcal{K} diverges. Since, $\rho^2 = a^2 \cos^2 \theta + r^2$ vanishes when simultaneously $r = 0$ and $\theta = \pi/2$, and recalling that $r = 0$ is not a point in space but a disc of radius a^2 , such that the set of points of the singularity is actually the ring at edge of $r = 0$. This can be seen more clearly in ellipsoidal coordinates; see Ref. [11] or Ref. [12] for details.

C. Maximal extension

The maximal extension for the spacetime (10) in the case when there are two horizons ($\beta_1^{\text{crit}} < \beta < \beta_2^{\text{crit}}$) can be obtained in a similar way to the case of the solution of Kerr-Newman [11,13]. We perform a transformation to Kerr coordinates $(r, \theta, u_{\pm}, \psi_{\pm})$, where

$$du_{\pm} = dt \pm \frac{r^2 + a^2}{Q(r)} dr, \quad d\psi_{\pm} = d\phi \pm \frac{a}{Q(r)} dr. \quad (26)$$

The metric takes the form

$$\begin{aligned} ds^2 = & \frac{[(r^2 + a^2)^2 - Qa^2 \sin^2 \theta]}{\rho^2} \sin^2 \theta d\psi_{\pm}^2 \\ & - \frac{(Q - a^2 \sin^2 \theta)}{\rho^2} du_{\pm}^2 \\ & - \frac{2a(a^2 + r^2 - Q)}{\rho^2} \sin^2 \theta du_{\pm} d\psi_{\pm} \\ & + \rho^2 d\theta^2 \pm 2du_{\pm} dr \mp 2a \sin^2 \theta dr d\psi_{\pm}. \end{aligned} \quad (27)$$

The maximal analytic extension is built up by a combination of the previous extensions as in the Kerr-Newman case. The global structure will be very similar to Kerr-Newman. Figure 3 shows the conformal structure of the solution (10). Three regions are permitted for the test particle movement, the regions *I* represent the regions asymptotically AdS which is $r > r_+$. Regions *II* ($r_- < r < r_+$) contain the trapped closed surfaces and finally regions *III* contain the ring singularity.

D. Electromagnetic fields

The electromagnetic potential A^μ can be written as a linear combination of two terms, $A_1(\theta)$ depending only on θ and $A_2(r)$ depending only on r ,

$$\begin{aligned} \rho^2 A_t &= f_1 a \cos \theta [1 + \beta a^2 \cos^2 \theta] + g_1 r (1 - \beta r^2) \\ &= A_1(\theta) + A_2(r), \\ \rho^2 A_\phi &= -\frac{a^2 + r^2}{a} A_1(\theta) - a \sin^2 \theta A_2(r), \end{aligned} \quad (28)$$

and $A_\theta = 0 = A_r$; the electromagnetic fields can be derived from them, being the nonvanishing components $F_{\theta t}, F_{r t}, F_{\theta \phi}, F_{r \phi}$. Asymptotically, at infinity, the electromagnetic fields behave as anti-de Sitter if $F_0 > 0$ or as de Sitter if $F_0 < 0$. However, if we assume physically reasonable energy conditions, there are the constraints that $\beta > 0$ and $F_0 > 0$ (see Ref. [4] for details on the energy conditions of this solution).

IV. MOTION OF CHARGED TEST PARTICLES IN THE STATIONARY NLE BH

Let us consider a charged test particle in the vicinity of the stationary NLE-BH; the test particle is characterized by a 4-velocity $u^\mu = dx^\mu/d\tau$, mass μ and charge q , with τ being an affine parameter. Since the spacetime is axisymmetric and stationary, associated with the existence of two Killing vectors, there are two conserved quantities, the energy E and the angular momentum L_z , related to the 4-velocity as

$$-E = \mu u_t + q A_t, \quad L_z = \mu u_\phi + q A_\phi. \quad (29)$$

It is then straightforward to determine $u^t = dt/d\tau = \dot{t}$ and $u^\phi = d\phi/d\tau = \dot{\phi}$; we define the functions $J(\theta)$ and $T(r)$, which involve the test particle parameters, as

$$\begin{aligned} J(\theta) &= a \tilde{L}_z - a^2 \sin^2 \theta \tilde{E} + \tilde{q} A_1(\theta), \\ T(r) &= -a \tilde{L}_z + (a^2 + r^2) \tilde{E} + \tilde{q} A_2(r), \end{aligned} \quad (30)$$

where the tilde denotes the parameter per unit mass of the test particle, $\tilde{x} = x/\mu$. In terms of $J(\theta)$ and $T(r)$, $dt/d\tau = \dot{t}$ and $d\phi/d\tau = \dot{\phi}$ can be written as

$$\begin{aligned} \rho^2 \dot{t} &= J(\theta) + \frac{r^2 + a^2}{Q(r)} T(r), \\ \rho^2 \dot{\phi} &= \frac{J(\theta)}{a \sin^2 \theta} + \frac{a T(r)}{Q(r)}. \end{aligned} \quad (31)$$

Using the Hamilton-Jacobi method, we can determine the remaining components of the test particle 4-velocity, \dot{r} and $\dot{\theta}$, in the stationary NLE BH. It turns out that the Hamilton-Jacobi equations are separable in the “ r ” and “ θ ” coordinates; this fact making manifest that a fourth

conserved quantity K exists in the Kerr-like spacetimes [14] that is the projection of the Killing tensor (also known as the Stäckel-Killing tensor), $K = K_{\mu\nu}\dot{x}^\mu\dot{x}^\nu$.

The action is written as

$$S = S_t + S_r + S_\theta + S_\phi - \frac{1}{2}\mu^2\tau. \quad (32)$$

Based on the mentioned symmetries, some components of the action can be written as

$$S_t = -Et; \quad S_\phi = L_z\phi. \quad (33)$$

Then the Hamilton-Jacobi equation is,

$$g^{\mu\nu}p_\mu p_\nu = g^{\mu\nu}[\partial_\mu S - qA_\mu][\partial_\nu S - qA_\nu] = -\mu^2, \quad (34)$$

where q is the charge of the test particle and A_μ are the electromagnetic potential components (28). Extending the sum in metric components, results in

$$g^{tt}(\partial_t S_t - qA_t)^2 + g^{rr}(\partial_r S_r)^2 + g^{\theta\theta}(\partial_\theta S_\theta)^2 + g^{\phi\phi}(\partial_\phi S_\phi - qA_\phi)^2 \quad (35)$$

$$+ 2g^{t\phi}(\partial_t S_t - qA_t)(\partial_\phi S_\phi - qA_\phi) = -\mu^2. \quad (36)$$

Substituting Eq. (33), we have the equation

$$g^{tt}(-E - qA_t)^2 + g^{rr}(\partial_r S_r)^2 + g^{\theta\theta}(\partial_\theta S_\theta)^2 + g^{\phi\phi}(L_z - qA_\phi)^2 + 2g^{t\phi}(-E - qA_t)(L_z - qA_\phi) = -\mu^2, \quad (37)$$

Substituting the contravariant components $g^{\mu\nu}$, Eqs. (13)–(17) into Eq. (37), we have

$$\begin{aligned} Q(r)(\partial_r S_r)^2 - \frac{1}{Q(r)}T(r)^2 + \mu^2 r^2 \\ = -K \\ = -(\partial_\theta S_\theta)^2 - \frac{1}{a^2 \sin^2 \theta}J(\theta)^2 - \mu^2 a^2 \cos^2 \theta. \end{aligned} \quad (38)$$

By separating variables, we end up with two equations, one depending on θ , the θ part, and the other one depending only on r , the r part, with K being the (Carter) separation constant:

$$(\partial_\theta S_\theta)^2 = K - \frac{1}{a^2 \sin^2 \theta}J(\theta)^2 - \mu^2 a^2 \cos^2 \theta, \quad (39)$$

$$Q(r)(\partial_r S_r)^2 = \frac{1}{Q(r)}T(r)^2 - \mu^2 r^2 - K. \quad (40)$$

It is known that $\partial_\mu S_\mu = p_\mu + qA_\mu = g_{\mu\nu}p^\nu + qA_\mu$, $p^\nu = m\dot{x}^\nu$ and since $A_r = 0 = A_\theta$, then $(\partial_\theta S_\theta)$ defines the motion in θ by the equation

$$\begin{aligned} (\rho^2 \dot{\theta})^2 &= \Theta(\theta) \\ &= \tilde{K} - a^2 \cos^2 \theta \\ &\quad - \frac{1}{a^2 \sin^2 \theta} [a\tilde{L}_z - a^2 \sin^2 \theta \tilde{E} + \tilde{q}A_1(\theta)]^2, \end{aligned} \quad (41)$$

where $\tilde{K} = K/\mu^2$.

Equation (41) is still coupled because the factor $\rho^2(r, \theta)$ arises on the left-hand side of the equation. To decouple it completely, we use the orbital parameter λ related with the proper time τ , also known as the Mino time and defined in Ref. [15], as

$$\frac{d\lambda}{d\tau} = \frac{1}{\rho^2}, \quad \tau = \int_0^\lambda \rho^2 d\lambda. \quad (42)$$

Note that the motion equations can be decoupled without introducing the Mino time [13], but using the Mino time decouples the radial and colatitudinal equations of motion in a simpler way. We present the forthcoming analysis in terms of functions dependent on the Mino time. The θ -motion equation can be written as

$$\frac{d\theta}{d\lambda} = \sqrt{\Theta(\theta)}. \quad (43)$$

The r part of the movement, from Eq. (38), is determined by the equation

$$\left(\frac{dr}{d\lambda}\right)^2 = T(r)^2 - Q(r)(\tilde{K} + r^2) = \mathcal{R}(r). \quad (44)$$

For the massless particle motion, we must take the limit $\mu = 0$ in Eqs. (39)–(40). Recall that massless test particle trajectories are not the trajectories followed by light rays, since in NLE the latter are governed by the null geodesics of an effective optical metric [16], which is determined from the NLE Lagrangian.

A. θ motion

Let us now consider the θ motion. From Eq. (41), we have a restriction for Θ : that is $\Theta \geq 0$ which is a general condition to guarantee motion in θ .

First of all, we list some general properties of the θ motion. From Eq. (41) note that the θ motion depends on the electromagnetic potential $A_1(\theta) = f_1 a \cos \theta (1 + \beta a^2 \cos^2 \theta)$ related to the magnetic charge of the BH and it has influence only over a charged test particle since it appears as the term $A_1 \tilde{q}$; then uncharged particles are not affected by the NLE field in their θ motion and it occurs qualitatively the same as in the Kerr-Newman geometry. Note also that the θ motion does not depend on the metric function $Q(r)$. Moreover there are some symmetries evident from Eq. (41):

- (i) Since the allowed regions for the θ motion demand that $\Theta \geq 0$, the Carter constant K must be positive since the subtracting terms in Eq. (41) are positive; then to have an allowed region requires a larger K than in the KN case ($\beta = 0$).
- (ii) A simultaneous change of sign of L_z and E is equivalent to a reflection on the equatorial plane: $\Theta|_{-L_z, -E}(\theta) = \Theta|_{L_z, E}(\pi - \theta)$.
- (iii) The movement in the equatorial plane, $\theta = \pi/2$ and $A_1 = 0$, is not allowed for arbitrary values of (E, L_z, a) but it may occur if $\tilde{K} - (a\tilde{E} - \tilde{L}_z)^2 \geq 0$, i.e., the Carter constant should be $K \geq (aE - L_z)^2$.
- (iv) A change of sign in qA_1 is equivalent to a reflection over the equatorial plane, $\Theta|_{-qf_1}(\theta) = \Theta|_{qf_1}(\pi - \theta)$.
- (v) One of the poles cannot be reached by test particles; which one is unreachable, $\theta = 0$ or $\theta = \pi$, depends on the sign of the product of the BH magnetic charge and the test particle charge f_1q . If $\tilde{q}f_1 > 0$ then the test particle cannot reach $\theta = 0$, while if $\tilde{q}f_1 < 0$ then $\theta = \pi$ is unreachable. Moreover in any case the test particle angular momentum L_z cannot be arbitrary (see Fig. 7), but it must hold that

$$(\tilde{q}A_1(\theta = 0, \pi) + a\tilde{L}_z) = 0.$$

Then $L_z = -qA_1(\theta = 0, \pi)/a$ or $L_z = 0 = q$.

Apart from the previous generalities, to examine the allowed regions for the motion in θ in terms of the BH and test particle parameters, we proceed to a change of variable from θ to x as follows:

$$x = \cos \theta, \quad (45)$$

with the range $-1 \leq x \leq 1$; the new variable x in terms of the old variable θ is

$$\dot{x} = -\dot{\theta} \sin \theta, \quad \dot{\theta} = -\sqrt{\Theta} \sin \theta. \quad (46)$$

Then Eq. (41) in terms of x , renders a sixth-degree polynomial,

$$\begin{aligned} \Theta(x) = & -x^6 a^2 q^2 \beta^2 f_1^2 - x^5 2a^3 \beta E f_1 q \\ & + x^4 a^2 (1 - E^2 - 2\beta q^2 f_1^2) \\ & + x^3 2a q f_1 [-E + a\beta(aE - L_z)] \\ & + x^2 [-K - f_1^2 q^2 - a^2 + 2aE(aE - L_z)] \\ & + x 2q f_1 (aE - L_z) - a^2 (aE - L_z)^2 + K, \end{aligned} \quad (47)$$

where the tilde $\tilde{}$ has been omitted, and the condition that $\Theta \geq 0$ defines the regions where the θ movement is available. The previous equation can be written as

$$\begin{aligned} \Theta = & -x^3 \beta a^2 q f_1 [\beta f_1 q x^3 + 2aE x^2 + 2f_1 q x - 2(aE - L_z)] \\ & + x^4 a^2 (1 - E^2) - x^3 2a q f_1 E \\ & + x^2 [-K - f_1^2 q^2 - a^2 + 2aE(aE - L_z)] \\ & + x 2q f_1 (aE - L_z) - a^2 (aE - L_z)^2 + K, \end{aligned} \quad (48)$$

where we have separated the nonlinear contribution in the first term; note that the nonlinear parameter appears combined as $a^2 \beta f_1 q$ and in general, we expect this term to be small since a is restricted to be less than the BH mass, as well as the magnetic (electric) BH charge; while the reduced test particle charge $\tilde{q} = q/m$ cannot be large, then the NLE effect in the θ motion is not very significant. In Figs. 4–8, we show the allowed regions, $\Theta(\theta) \geq 0$ when varying the parameters $\tilde{K}, \beta, a, \tilde{L}_z$, and \tilde{E} . Recall that the BH parameters are the mass, m , magnetic charge f_1 , electric charge, g_1 , and electromagnetic nonlinear parameter β , while the test particle parameters are the mass, μ , electric charge q , energy, \tilde{E} , the angular momentum projection onto the z axis, \tilde{L}_z , and the Carter constant K . The latter is associated with the total angular momentum: the total angular momentum of the test particle is not conserved and varies with θ , but the total angular momentum (BH angular momentum plus test particle angular momentum) must be conserved, so there is an exchange of angular momentum between the BH and the test particle, analogous to the KN case.

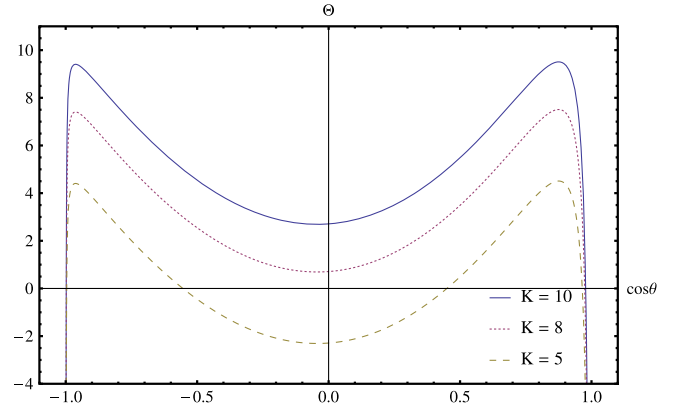


FIG. 4. The available regions for the bounded orbits in θ motion are shown for three values of the Carter constant K . The regions $\Theta \geq 0$ are the ones allowed for the motion of test particles and K must be large enough to make $\Theta \geq 0$; from top to bottom K decreases as $K = 10, 8$, and 5 . In this plot, we fix the parameters as $m = 1, a = 0.8, \beta = 5, f_1 = 0.5$ (BH magnetic charge), $\tilde{q} = 0.3, \tilde{E} = 4, \tilde{L}_z = 0.5$. Note that for these fixed parameters, if $\tilde{K} = 5$ there are two disconnected regions $\Theta > 0$, one above and the other below the equatorial plane where the test particle is allowed to move in bounded orbits, and there is a region not available for the test particle motion around the equatorial plane, $-0.5 < \cos \theta < 0.45$. Also note that the regions are not symmetrical with respect to the equatorial plane and that the allowed region does not include $\theta = 0$ ($\cos \theta = 1$).

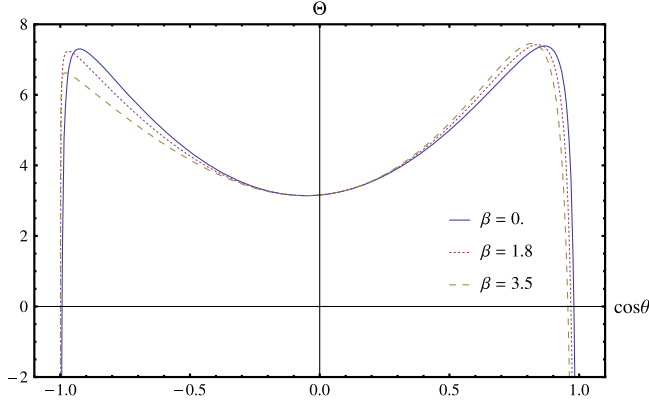


FIG. 5. The available regions for the bounded orbits in θ motion are shown for three values of the nonlinear parameter β , from top to bottom $\beta = 0, 1.8$, and 3.5 ; for fixed parameters the allowed regions are not very different from the KN-BH ($\beta = 0$); the situation is not different with a negative β . Note that even for $\beta = 0$ the allowed regions are not symmetrical respect to the equatorial plane ($\theta = \pi/2$) and as β increases the asymmetry is enhanced. In this plot, we fix the parameters as $m = 1, f_1 = 0.5$ (BH magnetic charge), $a = 0.9, \tilde{q} = 0.3, \tilde{K} = 8, \tilde{E} = 3, \tilde{L}_z = 0.5$.

From the plots, we see that depending on the values of the parameters the bounded movement in θ occurs in three types of regions: (i) the whole range $0 \leq \theta \leq \pi$, excepting one of the poles; (ii) in a strip defined by $\theta_{\min} < \theta < \theta_{\max}$; (iii) two disconnected regions, one above and the other below the equatorial plane, $\theta_1 < \theta < \theta_2$ and $\theta_3 < \theta < \theta_4$ where θ_i are positive real roots of $\Theta(\theta_i) = 0$, with general features described at the beginning of this section; in all cases one of the poles is unreachable. The movement in θ is determined by the BH magnetic charge, while the BH

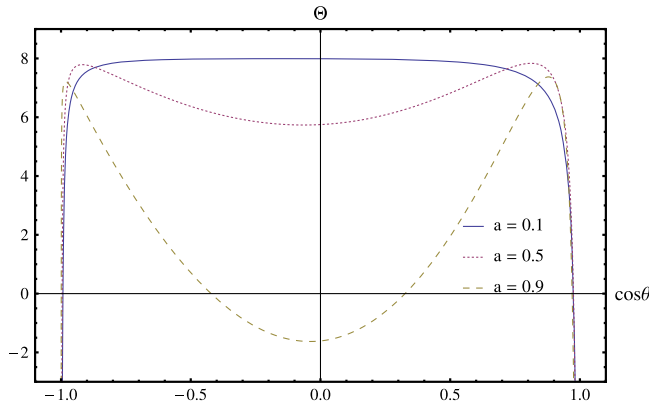


FIG. 6. The available regions for the bounded orbits in θ motion are shown for three values of the BH angular momentum, from top to bottom $a = 0.1, 0.5$, and 0.9 . For small values of a the motion is allowed almost in the whole θ range, and increasing a restricts the allowed region; see that for $a = 0.9$ the allowed region splits into two regions one of them above and the other below the equatorial plane. In this plot, we fix the parameters as $m = 1, f_1 = 0.5$ (BH magnetic charge), $\tilde{q} = 0.3, \beta = 2, \tilde{E} = 3, \tilde{L}_z = 0.5, K = 8$.

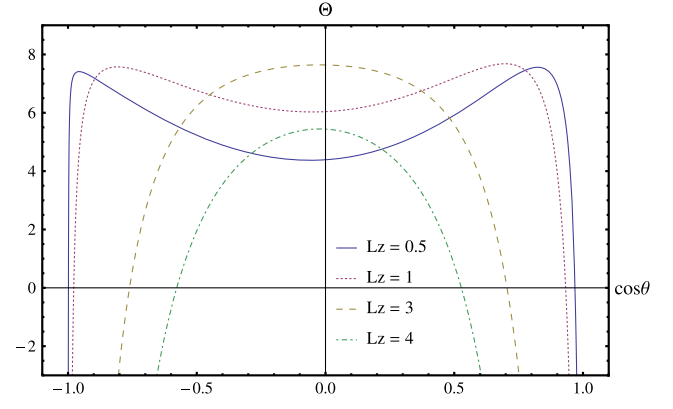


FIG. 7. The available regions for the bounded orbits in θ motion, $\Theta \geq 0$, are shown for different values of the test particle angular momentum \tilde{L}_z . The allowed regions decrease their θ range as L_z increases, for fixed values of the rest of the parameters; note that for large values of L_z the motion is constrained to a region near the equatorial plane. In this plot, we fix the parameters as $m = 1, a = 0.8, f_1 = 0.5$ (BH magnetic charge), $\beta = 2, \tilde{E} = 3, \tilde{q} = 0.3, \tilde{K} = 8$.

electric charge does not have any influence on this motion. Equation (41) for the linear (KN) limit obtained with $\beta = 0$ is a fourth-order polynomial given by

$$\begin{aligned} \Theta = & x^4(1 - E^2) - x^3 2qf_1 E \\ & + x^2[-K - f_1^2 q^2 - a^2 + 2aE(aE - L_z)] \\ & + x 2aqf_1(aE - L_z) - a^2((aE - L_z)^2 - K), \end{aligned} \quad (49)$$

which has been thoroughly studied by Hackmann in Ref. [17].

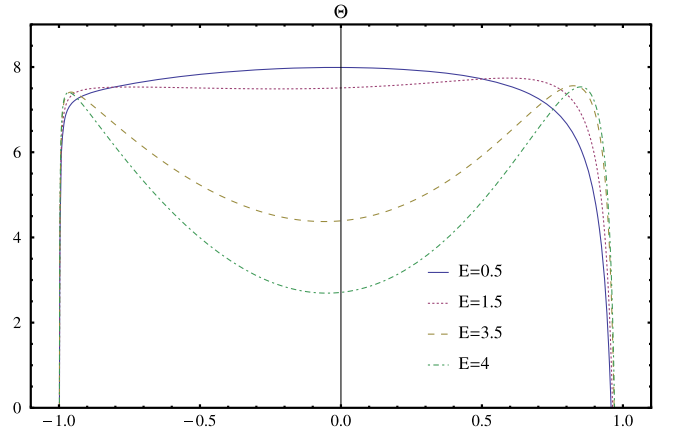


FIG. 8. The available regions for the bounded orbits in θ motion are shown for different values of the test particle energy \tilde{E} . The motion is allowed almost in the whole θ range, with the exception of the pole at $\theta = 0$; varying \tilde{E} changes the value of $d\theta/d\lambda$ at the equatorial plane ($\theta = \pi/2$), such that increasing \tilde{E} decreases the angular velocity of the test particle, $d\theta/d\lambda$ in the equatorial plane and its vicinity. In this plot, we fix the parameters as $m = 1, a = 0.8, \tilde{q} = 0.3, f_1 = 0.5$ (BH magnetic charge), $\beta = 5, \tilde{L}_z = 0.5, \tilde{K} = 8$.

B. r motion

The equation for the motion in r is Eq. (44), $\dot{r}^2 = \mathcal{R}(r)$, with $\mathcal{R}(r)$ given by,

$$\begin{aligned}\mathcal{R}(r) &= T(r) - (r^2 + \tilde{K})Q(r) \\ &= [\tilde{q}A_2(r) - a\tilde{L}_z + \tilde{E}(r^2 + a^2)]^2 - (r^2 + \tilde{K})Q(r),\end{aligned}$$

$$\begin{aligned}\mathcal{R}(r) &= \beta^2(g_1^2q^2 - F_0)r^6 - 2\beta E g_1 q r^5 + [E^2 - 1 - \beta^2 F_0 K + 2\beta(F_0 - g_1^2 q^2)]r^4 + [2m + 2g_1 q(E + a\beta(L_z - aE))]r^3 \\ &\quad + [g_1^2 q^2 + 2aE(aE - L_z) - K(1 - 2\beta F_0) - a^2 - F_0]r^2 + (K2m + 2a g_1 q(aE - L_z))r \\ &\quad + a^2(aE - L_z)^2 - K(a^2 + F_0).\end{aligned}\tag{50}$$

The previous Eq. (50) with $\beta = 0$, making $F_0 = Q_e^2$ and $g_1 = Q_e$, where Q_e is the BH electric charge, we recover the KN case

$$\begin{aligned}\mathcal{R}^{KN}(r) &= (E^2 - 1)r^4 + [2m + 2Q_e q E]r^3 \\ &\quad + [Q_e^2(q^2 - 1) + 2aE(aE - L_z) - K - a^2]r^2 \\ &\quad + (K2m + 2aQ_e q(aE - L_z))r \\ &\quad + a^2(aE - L_z)^2 - K(a^2 + Q_e^2),\end{aligned}\tag{51}$$

which is a fourth-degree polynomial. Then $\mathcal{R}^{KN}(r) = 0$ has two real roots, one positive and one negative and two complex conjugate roots. One of the differences observed in the stationary NLE BH is that, for the same fixed parameters, $\mathcal{R} = 0$ has four real roots, two positive and two negative, in addition to two complex conjugate roots. The two positive roots are the turning points and the radius that delimit the region of bounded orbits. This region could be connected to a more efficient creation of an accretion disk around the BH. Therefore the stationary NLE is a BH that will more easily capture test particles, then pointing to a more efficient creation of an accretion disk around the BH. One of the positive roots is in the interior of the BH, and the larger radius of the turning points defines the region of the bounded orbits. Geodesics of the KN spacetime were analyzed in Ref. [17]; see also Ref. [18].

In the next subsection, we describe how Eq. (44) can be integrated.

C. Solution in terms of hyperelliptic functions

The radial coordinate in Eq. (44) can be integrated as

$$\lambda = \int \frac{dr}{\sqrt{\mathcal{R}(r)}}.\tag{52}$$

If we knew a zero of $\mathcal{R}(r_0) = 0$ (which might be a circular orbit radius or a turning point), then we could

and the NLE contribution is through the parameter β in the electromagnetic potential $A_2(r) = g_1 r(1 - \beta r^2)$ and the metric function $Q(r) = \kappa F_0(1 - \beta r^2)^2/2 - 2mr + r^2 + a^2$; in what follows we omit the tilde \tilde{x} and fix $\kappa = 1$. The turning points, where $\dot{r} = 0$, are given by the roots of $\mathcal{R} = 0$ and since $Q(r)$ is a fourth-order polynomial, \mathcal{R} is a sixth-order polynomial in r , given by

reduce the degree of \mathcal{R} by substituting $r \mapsto 1/x + r_0$. The resulting fifth-degree polynomial, \mathcal{R}_x , is given by

$$\mathcal{R}_x = \sum_{j=0}^5 \frac{a_j}{a_5} x^j, \quad a_j = \frac{(\pm 1)^j}{(6-j)!} \left. \frac{d^{(6-j)} \mathcal{R}}{dr^{(6-j)}} \right|_{r_0}.\tag{53}$$

This leads to the hyperelliptic differential equation of the first kind,

$$x \frac{dx}{d\lambda} = E \sqrt{a_5 \mathcal{R}_x}.\tag{54}$$

The equations involving hyperelliptic Riemann surfaces of genus 2 and one relevant degree of freedom are integrated in the framework of the Jacobi inversion problem, using a reduction to the θ divisor (Jacobi theta function) on the Jacobi variety, i.e., to the set of zeros of the θ function. The explicit solutions are given in terms of the Kleinian σ functions and their derivatives; therefore the solution for $r(\lambda)$ is given by

$$r(\lambda) = \mp \frac{\sigma_2}{\sigma_1} \left(\begin{array}{c} f(\tau - \tau'_0) \\ \tau - \tau'_0 \end{array} \right) + r_0,\tag{55}$$

where $\sigma_i, i = 1, 2$ are the derivatives of the Kleinian σ function and f describes the θ divisor, i.e., $\sigma((f(z), z)') = 0$. The same procedure can be applied to the equation for the θ motion which is also a sixth-degree polynomial in $x = \cos \theta$. This method applied to particle motion in general relativity was introduced in Refs. [19–21]. Therefore, in principle, the analytic solutions can be determined; however in this contribution we will content ourselves with a qualitative description of the possible test particle bounded orbits.

D. Effective potential

Equation (50) is a quadratic equation in E , which can be written in terms of two effective potentials $V_{\text{eff}\pm}$ as

$$\mathcal{R}(r) = (E - V_{\text{eff}+})(E - V_{\text{eff}-}),$$

$$V_{\text{eff}\pm} = \frac{1}{(r^2 + a^2)} \{ (aL_z - qA_2(r)) \pm \sqrt{Q(r)(K + r^2)} \}.$$

The positive square root is the one that corresponds to a 4-momentum pointing toward the future. Since $V_{\text{eff}-}$ can be negative then a region exists from which energy can be extracted by a Penrose process; that region is called the effective ergoregion [22]. For a stationary charged BH the energy extraction can be at the expense of electromagnetic energy or rotational energy. In Figs. 9–10, we plot the effective potentials for positive and negative F_0 , and for different values of β , respectively. The available regions for the motion of the test particle are the regions above and below the curves; maxima and minima can be seen, which indicates that there are both unstable and stable circular orbits (where $V'_{\text{eff}} = 0$).

E. Circular orbits

The spherical orbits are defined by $\mathcal{R} = 0$ and $\mathcal{R}' = 0$. This last condition is given by

$$\begin{aligned} \mathcal{R}' = & 6\beta^2(g_1q^2 - F_0)r^5 - 10\beta E g_1 q r^4 \\ & + 4[E^2 - 1 - \beta^2 F_0 K + 2\beta(F_0 - g_1^2 q^2)]r^3 \\ & + 3[2m + 2g_1q(E + a\beta(L_z - aE))]r^2 \\ & + 2[g_1^2 q^2 + 2aE(aE - L_z) - K - a^2 - (1 - 2\beta K)F_0]r \\ & + (K2m + 2ag_1q(aE - L_z)) = 0. \end{aligned} \quad (56)$$

From the two conditions, $\mathcal{R} = 0$ and $\mathcal{R}' = 0$, we can derive the condition for the circular orbits as

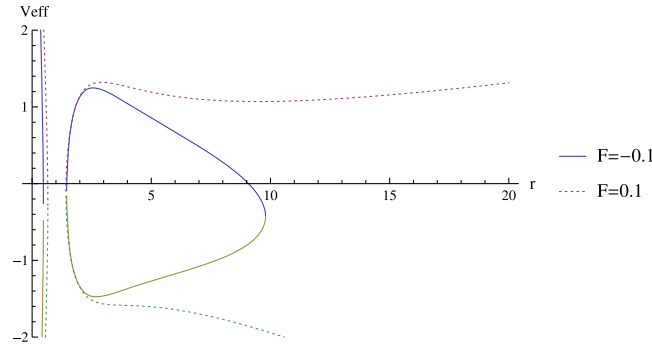


FIG. 9. The curves show the effective potentials $V_{\text{eff}\pm}$ for $F_0 = -0.2, 0.2$. The area between the curves is forbidden for the motion of the test particle. Note that $V_{\text{eff}-}$ can be negative; then the possibility exists of energy extraction by means of the Penrose process. In this plot, we fix the parameters as $m = 1$, $a = 0.9$, $\tilde{q} = 0.3$, $g_1 = 0.5$ (BH magnetic charge), $\beta = 0.3$, $\tilde{L}_z = 0.5$, $\tilde{K} = 40$.

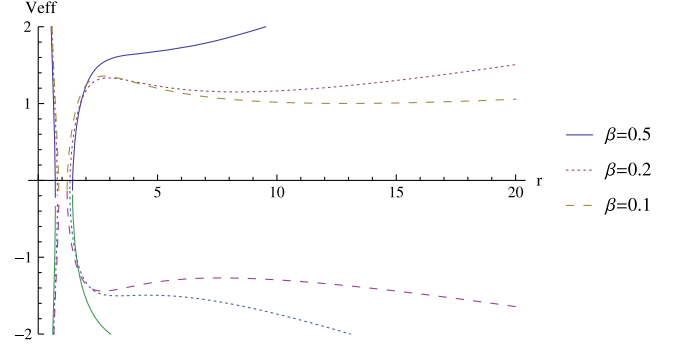


FIG. 10. The effective potentials $V_{\text{eff}\pm}$ are shown for three different values of β . The area between the curves is forbidden for the movement of the test particle. In this plot, we fix the parameters as $m = 1$, $a = 0.9$, $\tilde{q} = 0.3$, $g_1 = 0.5$ (BH magnetic charge), $F_0 = 0.2$, $\tilde{L}_z = 0.5$, $\tilde{K} = 40$. There exist both maxima and minima then unstable and stable circular orbits occur; as β increases no minima occur, then no circular orbits are present for $\beta > 0.5$, for the chosen values of parameters in this plot.

$$4(qA_2' + 2rE)^2 Q(r)(r^2 + K) - (2rQ(r) + Q(r)'(r^2 + K^2))^2 = 0, \quad (57)$$

where $f' = df(r)/dr$. Numerical solutions can be found for this equation, showing that indeed circular orbits can exist in the vicinity of this black hole. In Figs. 11 and 12, we show the radius of the circular orbits r_c for fixed

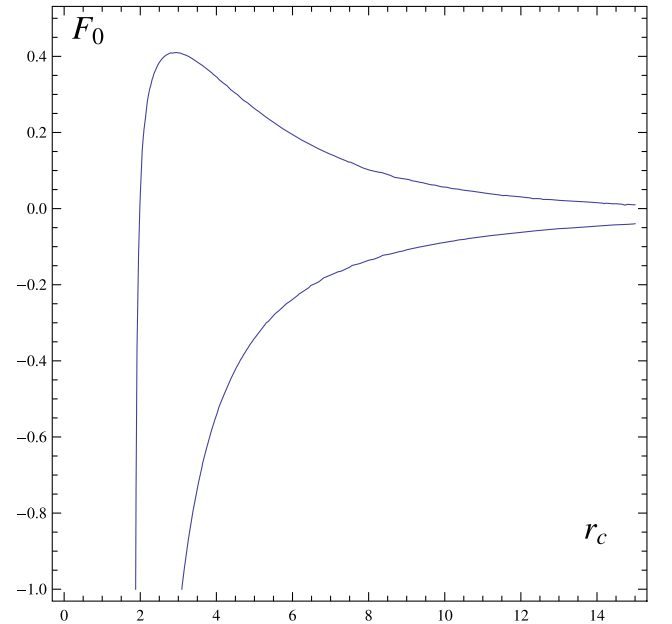


FIG. 11. The curve shows F_0 (related to the BH charge) as a function of the radius of the circular orbits r_c . In this plot, we fix the parameters as $m = 1$, $a = 0.9$, $\tilde{q} = 0.3$, $g_1 = 0.5$ (BH electric charge), $\beta = 0.3$, $\tilde{L}_z = 0.5$, $\tilde{K} = 40$. There are values of $F_0 > 0$ that allow two circular orbits while none exist for $F_0 > 0.43$.

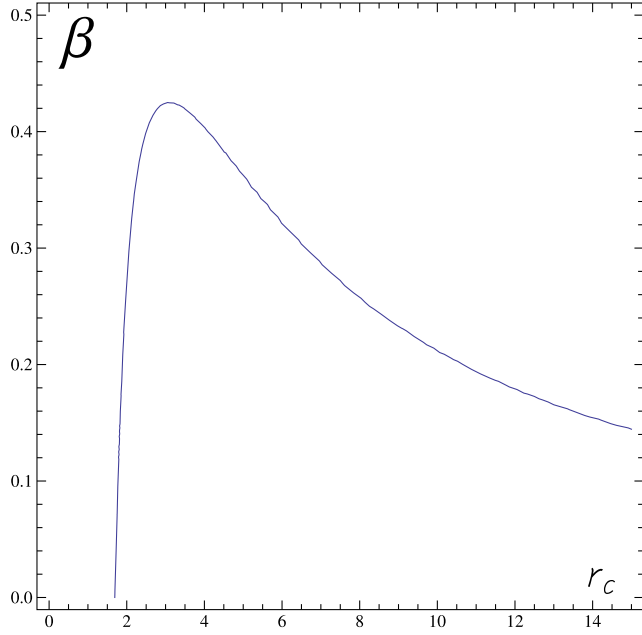


FIG. 12. The curve shows the NLE parameter β as a function of the radius of the circular orbits r_c . In this plot, we fix the parameters as $m = 1, a = 0.9, \tilde{q} = 0.3, g_1 = 0.5$ (BH electric charge), $F_0 = 0.2, \tilde{L}_z = 0.5, \tilde{K} = 40$. Note that there are two circular orbits for β in the range $0.14 < \beta < 0.43$ and there are no circular orbits for $\beta > 0.43$. In the case KN, $\beta = 0$, there is only one circular orbit.

parameters and varying β and F_0 . Note that there are two possible circular orbits for most of the ranges, indicating that unstable and stable circular orbits may occur, in agreement with the effective potential shape. Moreover, the circular orbits of the stationary NLE-BH have a greater radius than the KN one.

F. Bounded orbit regions, $\mathcal{R} \geq 0$

In Fig. 13 the generic behavior of \mathcal{R} is illustrated for the KN ($\beta = 0$) and for the stationary NLE BH ($\beta = 0.5$). For a qualitative description of the test particle motion, we have explored the regions in which bounded orbits can occur, $\mathcal{R} \geq 0$, by varying the parameters. Moreover, $\mathcal{R} = \dot{r}^2 = 0$ at the turning points and the effect of varying the parameters modifies the position of the turning points: if the turning point is closer to the horizon, then the region with bounded orbits is smaller, and vice versa. In Figs. 14–19, we explore the allowed regions (only the regions of interest $r \geq 0$ are shown), first varying the test particle parameters \tilde{L}_z, \tilde{E} and \tilde{q} :

- (i) Increasing \tilde{L}_z the turning point is closer to the horizon, then the allowed region for bounded orbits, $\mathcal{R}(r) \geq 0$ is smaller; see Fig. 14.
- (ii) As \tilde{E} increases the allowed region $\mathcal{R}(r)$ is enlarged and the turning point is farther from the horizon. For $\tilde{E} < 1$ that the test particle cannot stay in the

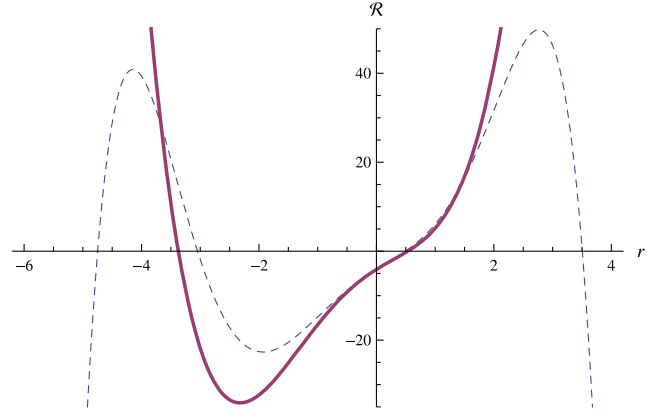


FIG. 13. The generic behavior of the function \mathcal{R} is illustrated for the (continuous) KN ($\beta = 0$) and for the (dashed) stationary NLE BH ($\beta = 0.5$). For the KN BH $\mathcal{R} = 0$ has two real roots, one positive and one negative, while the stationary NLE BH $\mathcal{R} = 0$ has four real roots, two positive and two negative, in addition to the two complex conjugate roots. The two positive roots are the turning points and the radius that delimit the region of bounded orbits. This region is related to the BH capacity of growing an accretion disk. In this plot the parameters are fixed as $m = 1, \tilde{L}_z = 0.5, \tilde{q} = 0.3, \tilde{K} = 4, a = 0.9, F_0 = 0.36, g_1 = 0.6, E = 1.5$.

forbidden regions in the vicinity of the black hole, i.e., $\mathcal{R} < 0$; see Fig. 15. In the absence of positive real roots the orbits are of transit type: the particle starts at $\pm\infty$, comes to a point of closest approach, $r = r_o$ and then goes back to infinity.

- (iii) As \tilde{q} decreases the allowed region $\mathcal{R}(r)$ is enlarged since the turning point is farther from the horizon. The maximum allowed region is for the uncharged test particle, $\tilde{q} = 0$; see Fig. 16.

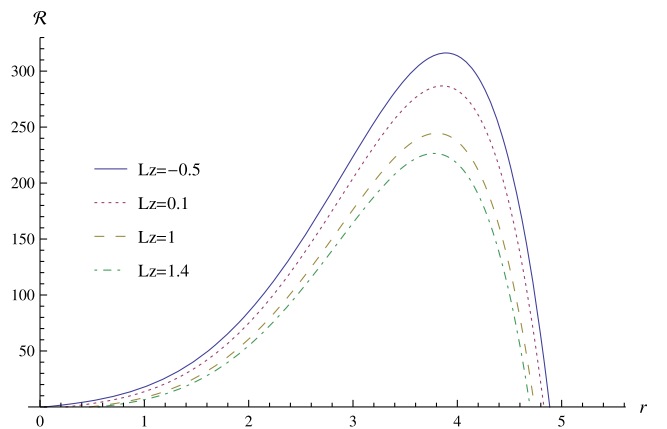


FIG. 14. The allowed regions for bounded orbits, $\mathcal{R} \geq 0$, are shown for different values of the test particle angular momentum, from top to bottom $\tilde{L}_z = -0.5, 0.1, 1, 4$; the allowed region decreases as \tilde{L}_z increases. The rest of the parameters are fixed as $m = 1, \tilde{E} = 2, \tilde{q} = 0.3, \tilde{K} = 4, m = 1, a = 0.9, \beta = 0.5, F_0 = 0.36, g_1 = 0.6$.

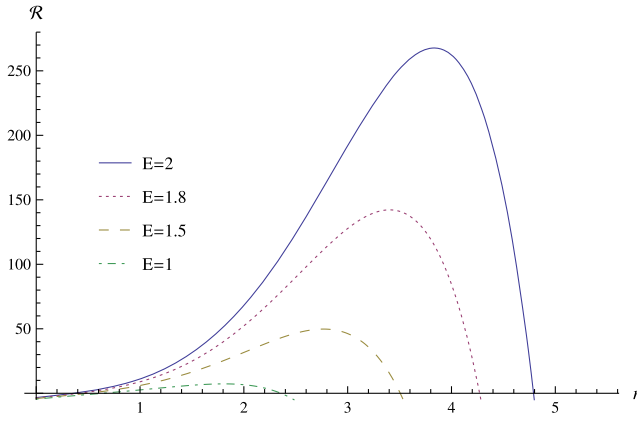


FIG. 15. It is shown \mathcal{R} as a function of r ; the allowed regions for bounded orbits, $\mathcal{R} \geq 0$, are shown for different values of the test particle energy, from top to bottom $\tilde{E} = 2, 1.5$, and 1 ; the allowed region increases as E augments; note that for $E < 1$ no bounded orbits are possible. The rest of the parameters are fixed as $m = 1$, $\tilde{L}_z = 0.5$, $\tilde{q} = 0.3$, $\tilde{K} = 4$, $a = 0.9$, $\beta = 0.5$, $F_0 = 0.36$, $g_1 = 0.6$.

Now by varying the black hole parameters a , Q , β , we obtain the following behaviors:

- (i) As a increases the allowed region $\mathcal{R}(r)$ is enlarged and the turning point is farther from the horizon; regions are not very different when varying a ; see Fig. 17.
- (ii) Increasing the BH charge, $g_1 = Q_e$, makes the turning point be nearer the horizon and the allowed region $\mathcal{R}(r)$ becomes smaller. For the uncharged (Kerr) BH, $Q_e = 0$ there are not positive real roots, then the orbits are of transit type; see Fig. 18.
- (iii) As β decreases the allowed region $\mathcal{R}(r)$ is enlarged or the turning point is farther from the horizon. For the linear electromagnetic case, $\beta = 0$ there are not

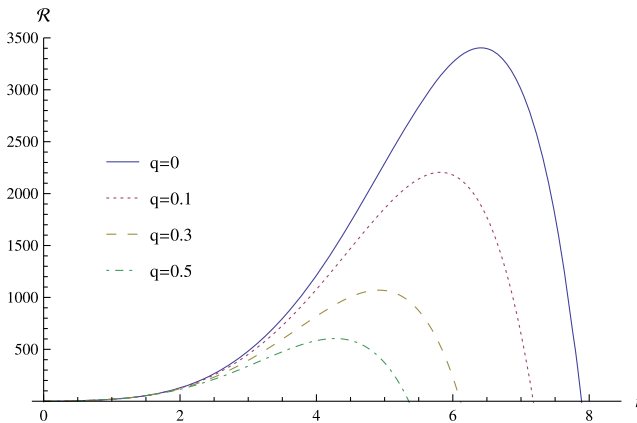


FIG. 16. The regions allowed for a bounded test particle motion, $\mathcal{R} \geq 0$, are shown for different values of the test particle charge $\tilde{q} = q/m$. The rest of the parameters are fixed as $m = 1$, $E = 2.5$, $\tilde{L}_z = 0.3$, $\tilde{K} = 4$, $M = 1$, $a = 0.9$, $\beta = 0.5$, $F_0 = 0.36$, $g_1 = 0.6$. The uncharged particle has the largest allowed region.

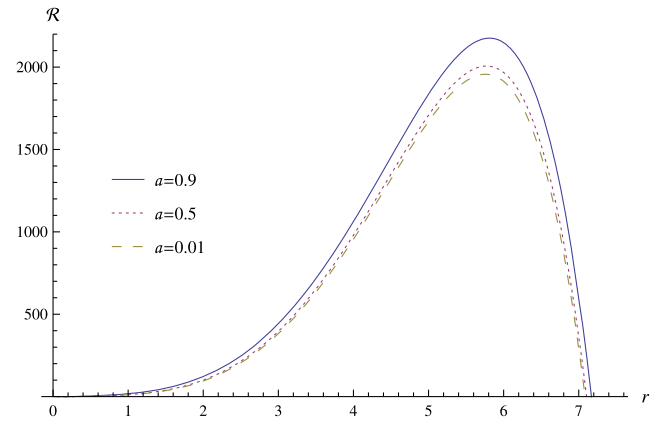


FIG. 17. The allowed regions for bounded orbits, $\mathcal{R} \geq 0$, are shown for different values of the BH angular momentum. From top to bottom $a = 0.9, 0.5, 0.3$, and 0.1 ; as a decreases the allowed region gets smaller but the reduction is not substantial. The rest of the parameters are fixed as $m = 1$, $\tilde{E} = 2.5$, $\tilde{q} = 0.1$, $\tilde{L}_z = 0.5$, $\beta = 0.5$, $F_0 = 0.36$, $g_1 = 0.6$.

positive real roots, then the orbits are of transit type; see Fig. 19.

G. ϕ motion

We first note that the possibility exists for a test particle coming with a certain angular momentum, that it reverses its motion; i.e., it may happen that $\dot{\phi} = 0$, the equation that determine the corresponding θ angle is

$$P(x)Q(r) + (a^2 - x^2)T(r) = 0, \quad (58)$$

where $x = a \cos \theta$ that is a third-degree polynomial. Otherwise the motion resembles the KN one.

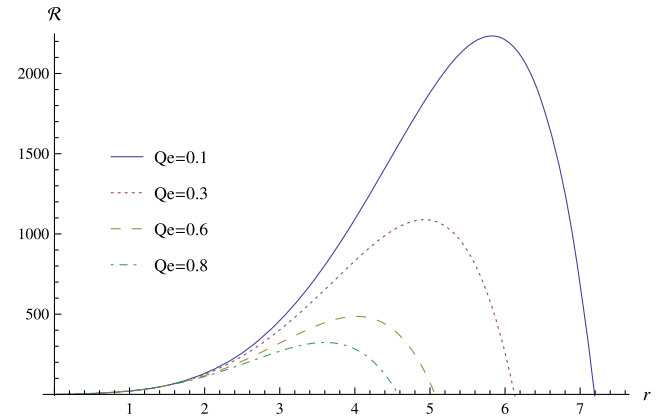


FIG. 18. It is shown \mathcal{R} as a function of r , for different values of the BH electric charge $g_1 = Q_e = 0.1, 0.5, 0.6$, and 0.8 ; the allowed regions for bounded orbits, $\mathcal{R} \geq 0$, decrease as Q_e increases; for the uncharged BH (not shown in this plot) there are not test particle bounded orbits. The rest of the parameters are fixed as $m = 1$, $\tilde{E} = 2.5$, $\tilde{q} = 0.1$, $\tilde{L}_z = 0.5$, $\tilde{K} = 4$, $a = 0.9$, $\beta = 0.5$, $F_0 = 0.36$.

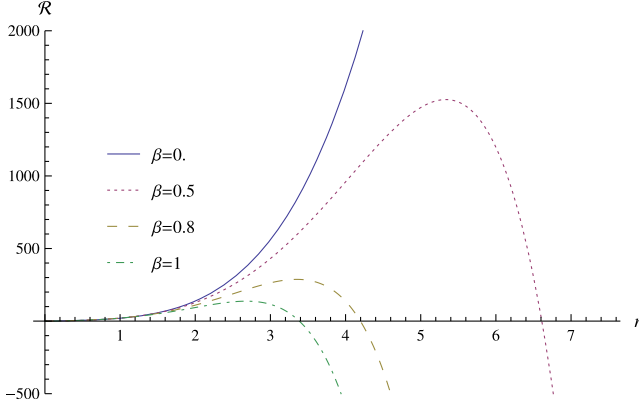


FIG. 19. The allowed regions for bounded orbits, $\mathcal{R} \geq 0$, are shown for different values of the nonlinear electromagnetic parameter β , from top to bottom $\beta = 0, 0.5, 0.8$, and 1 ; increasing β decreases the allowed region $\mathcal{R} > 0$. The rest of the parameters are fixed as $m = 1, \tilde{E} = 2.5, \tilde{q} = 0.1, \tilde{L}_z = 0.5, \tilde{K} = 4, a = 0.9, F_0 = 0.36, g_1 = 0.6$. For $\beta = 0$ there are no bounded orbits.

V. BIREFRINGENCE

To consider the massless particles motion, we must take the limit $\mu = 0$ in Eqs. (39)–(40). Recall that massless test particle trajectories are not the trajectories followed by light rays, since in NLE these are governed by the null geodesics of an effective optical metric [16], which is determined by the NLE Lagrangian. In fact birefringence occurs in nonlinear electrodynamics with the exception of the Born-Infeld (BI) theory [16]; the propagation of signals in BI theory was studied in Ref. [23].

Given a Lagrangian depending on the two electromagnetic invariants F and G , $L(F, G)$, there are two effective optical metrics $\gamma^{(1,2)\mu\nu}$ given in terms of derivatives of the Lagrangian respect F and G ; these are,

$$\begin{aligned} \gamma^{(1)\mu\nu} &= (L_F - 2L_{GG}F)g^{\mu\nu} - 4L_{GG}F_{,\lambda}^{\mu}F^{\lambda\nu}, \\ \gamma^{(2)\mu\nu} &= L_F g^{\mu\nu} - 4L_{FF}F_{,\lambda}^{\mu}F^{\lambda\nu}, \end{aligned} \quad (59)$$

where $g^{\mu\nu}$ is the spacetime metric, in our case the stationary NLE-BH. For Maxwell electrodynamics, $L(F) = F$, $\gamma^{(1)\mu\nu} = \gamma^{(2)\mu\nu} = g^{\mu\nu}$ and birefringence does not occur. Therefore in the spacetime of the stationary NLE-BH birefringence will take place and we can determine the two effective optical metrics from Eq. (59) by means of the chain rule, since we know the derivatives of the Lagrangian with respect to the coordinates r and θ . Although straightforward, the procedure is cumbersome; for instance the expression for L_{FF} becomes

$$\begin{aligned} L_{FF} &= 2 \frac{L_{,r\theta}}{F_{,r}F_{,\theta}} - \frac{F_{,r\theta}}{F_{,r}F_{,\theta}} \left[\frac{L_{,\theta}}{F_{,\theta}} + \frac{L_{,r}}{F_{,r}} \right] \\ &+ \frac{1}{F_{,r}^2} \left[L_{,rr} - \frac{L_{,r}F_{,rr}}{F_{,r}} \right] + \frac{1}{(F_{,\theta})^2} \left[L_{,\theta\theta} - \frac{L_{,\theta}F_{,\theta\theta}}{F_{,\theta}} \right]. \end{aligned} \quad (60)$$

The rest of the derivatives, L_F, L_{GG} , can be determined analogously since, we do know the Lagrangian and the electromagnetic invariants as functions of (r, θ) .

Undoubtedly it would be interesting to determine the light trajectories in this metric; however we leave it for future research.

VI. CONCLUSIONS

We have studied the properties of the stationary axisymmetric nonlinear electromagnetic spacetime that generalizes the Kerr-Newman BH. The solution possesses mass, rotation, electric and magnetic charges and three parameters associated with the NLE: β of the electromagnetic potentials and F_0, G_0 related to the BH electric and magnetic charges. From the analysis, we conclude the following.

The sign of the nonlinear parameter F_0 determines the asymptotics of the spacetime: de Sitter if $F_0 < 0$ and anti-de Sitter when $F_0 > 0$. While the value of β determines the number of horizons, being then two critical values β_1 and β_2 , for which there is only one horizon; if $\beta < \beta_1$ no horizons occur as well as if $\beta > \beta_2$; and for $\beta_1 < \beta < \beta_2$ the BH presents two horizons; in addition, if $F_0 < 0$ there is the cosmological horizon.

From the Kretschmann invariant, we see that the introduction of the NLE field affects the curvature. Assuming $\beta > 0$ and $F_0 > 0$ (in agreement with physically reasonable energy conditions) the stationary NLE BH curvature is larger than that of KN; accordingly, the bounded orbits are closer to the horizon for the rotating NLE BH than for KN.

For the motion of a charged test particle, the Hamilton-Jacobi equations turn out to be separable, and likewise for the Kerr-Newman case, and in principle analytic solutions can be derived for the geodesic equations for θ and r , related to a sixth-degree polynomial. We did not follow that path and instead described the regions allowed for the bounded motion of a charged test particle by varying the parameters; the allowed regions are illustrated in the plots for $\Theta(\theta) \geq 0$ and $\mathcal{R}(r) \geq 0$. Among the effects of the introduction of the NLE field are the shrinking of the regions allowed for test particle bounded orbits. The allowed regions in terms of θ are defined by the positive real roots of $\Theta(\theta) = 0$, and there are three possible cases: (i) the whole range $0 < \theta < \pi$, except one of the poles; (ii) a strip defined by a $\theta_{\min} < \theta < \theta_{\max}$; (iii) two disconnected regions, one above and the other below the equatorial plane; in all cases one of the poles is unreachable. The relative signs of the magnetic charge and the charge of the test particle determine which one of the poles is unreachable: if $\tilde{q}f_1 > 0$ then the test particle cannot reach $\theta = 0$, while if $\tilde{q}f_1 < 0$ then $\theta = \pi$ is unreachable.

For the radial motion circular orbits appear in agreement with the shape of the effective potential that presents maxima and minima. There is also the possibility of energy extraction since the effective potentials have regions of

negative values. In general the r motion is qualitatively the same as in KN spacetime but some differences arise: the NLE parameter modifies the number of bound orbits and there exists a second circular orbit outside the horizon. The regions allowed for the test particle bounded orbits are closer to the horizon if the NLE parameter β increases and are larger for the uncharged BH (Kerr case). Augmenting the BH charge, the test particle charge or the nonlinear parameter β results in a smaller radius for the turning points that delimits the regions of bounded orbits; as a consequence, the stationary NLE BH may increase its accretion disk more easily.

The birefringence effect takes place in this spacetime and it is explained how to obtain the effective optical metrics that determine light trajectories in this NLE spacetime.

ACKNOWLEDGMENTS

N.B. acknowledges partial support by the Consejo Nacional de Ciencia y Tecnología (CONACYT)-Project No. 284489. G.G.-C. acknowledges the support from CONACYT, Mexico, Estancias Posdoctorales por México 2021, Grant No. 1031130.

APPENDIX: ROOTS

The metric function representing a rotating charged black hole with nonlinear electrodynamics in a Kerr-like spacetime is

$$Q(r) = \frac{\kappa F_0}{2} (1 - \beta r^2)^2 - 2mr + r^2 + a^2, \quad (\text{A1})$$

which we rewrite as follows as:

$$Q(r) = A_1 r^4 + A_2 r^2 + A_3 r + A_4, \quad (\text{A2})$$

where A_i are the coefficients defined as

$$\begin{aligned} A_1 &= \frac{\kappa F_0 \beta^2}{2}, & A_2 &= 1 - \kappa F_0 \beta, \\ A_3 &= -2m, & A_4 &= \frac{\kappa F_0}{2} + a^2. \end{aligned} \quad (\text{A3})$$

According to the Cardano-Ferrari method it is possible to determine analytical expressions for a fourth-degree polynomial. The roots of Eq. (A2) are

$$r_{1,2} = \frac{1}{2} \sqrt{-\frac{2A_2}{3A_1} + \mathcal{B}} \mp \frac{1}{2} \sqrt{-\frac{4A_2}{3A_1} - \mathcal{B} - \frac{2A_3}{A_1 \sqrt{-\frac{2A_2}{3A_1} + \mathcal{B}}}}, \quad (\text{A4})$$

and

$$r_{3,4} = -\frac{1}{2} \sqrt{-\frac{2A_2}{3A_1} + \mathcal{B}} \mp \frac{1}{2} \sqrt{-\frac{4A_2}{3A_1} - \mathcal{B} + \frac{2A_3}{A_1 \sqrt{-\frac{2A_2}{3A_1} + \mathcal{B}}}}, \quad (\text{A5})$$

where \mathcal{B} is defined as

$$\mathcal{B} = \frac{2^{1/3}(A_2^2 + 12A_1A_4)}{3A_1\mathcal{A}} + \frac{\mathcal{A}}{3(2)^{1/3}A_1}, \quad (\text{A6})$$

and we define \mathcal{A} as

$$\begin{aligned} \mathcal{A}^3 &= 2A_2^3 + 27A_1A_3^2 - 72A_1A_2A_4 \\ &+ \sqrt{-4(A_2^2 + 12A_1A_4)^3 + (2A_2^3 + 27A_1A_3^2 - 72A_1A_2A_4)^2}. \end{aligned}$$

-
- [1] B. P. Abbot *et al.* (LIGO Scientific and Virgo Collaborations), Tests of General Relativity with GW150914, *Phys. Rev. Lett.* **116**, 221101 (2016).
- [2] B. P. Abbot *et al.* (LIGO Scientific, Virgo Collaborations and KAGRA Collaboration), GWTC-3: Compact binary coalescences observed by LIGO and Virgo during the second part of the third observing run, [arXiv:2111.03606](https://arxiv.org/abs/2111.03606).
- [3] A. A. García-Díaz and G. Gutierrez-Cano, Linear superposition of regular black hole solutions of Einstein nonlinear electrodynamics, *Phys. Rev. D* **100**, 064068 (2019).
- [4] A. A. García-Díaz, Stationary rotating black hole exact solution within Einstein-nonlinear electrodynamics, [arXiv:2112.06302](https://arxiv.org/abs/2112.06302).
- [5] A. A. García-Díaz, AdS-dS stationary rotating black hole exact solution within Einstein-nonlinear electrodynamics, *Ann. Phys. (Amsterdam)* **441**, 168880 (2022). Note that Eq. (90) for $Q(r)$ contains an extra factor F_0 in its first term while in μ from Eq. (111) the Λ term is spurious.
- [6] H. Salazar, A. Garcia, and J. F. Plebański, Duality rotations and type D solutions to Einstein equations with nonlinear electrodynamics sources, *J. Math. Phys. (N.Y.)* **28**, 2171 (1987).
- [7] M. Born and L. Infeld, Foundations of a new field theory, *Proc. R. Soc. A* **144**, 125 (1934).
- [8] The roots of the polynomial are shown explicitly in Appendix.
- [9] R. Torres and F. Fayos, On regular rotating black holes, *Gen. Relativ. Gravit.* **49**, 2 (2017).
- [10] A. A. Garcia-Diaz and G. Gutierrez-Cano, Regularity conditions for spherically symmetric solutions of Einstein-nonlinear electrodynamics equations, *Ann. Phys. (Amsterdam)* **422**, 168323 (2020).

- [11] S. W. Hawking and G. F. E. Ellis, *The Large Scale Structure of Space-Time* (Cambridge University Press, Cambridge, England, 1973).
- [12] S. M. Carroll, *Spacetime and Geometry* (Addison-Wesley, Reading, MA, 2004).
- [13] B. Carter, Global structure of the Kerr family of gravitational fields, *Phys. Rev.* **174**, 1559 (1968).
- [14] M. Visinescu, Higher order first integrals, Killing tensors and Killing-Maxwell system, *J. Phys. Conf. Ser.* **343**, 012126 (2012).
- [15] Y. Mino, Perturbative approach to an orbital evolution around a supermassive black hole, *Phys. Rev. D* **67**, 084027 (2003).
- [16] S. Alarcon Gutierrez, A. L. Dudley, and J. F. Plebański, Signals and discontinuities in general relativistic non-linear electrodynamics, *J. Math. Phys. (N.Y.)* **22**, 2835–48 (1981).
- [17] E. Hackmann and Hongxiao Xu, Charged particle motion in Kerr-Newmann space-times, *Phys. Rev. D* **87**, 124030 (2013).
- [18] H. Cebeci, N. Ozdemir, and S. Sentorun, Motion of the charged test particles in Kerr-Newman-Taub-NUT space-time and analytical solutions, *Phys. Rev. D* **93**, 104031 (2016).
- [19] V. Enolskii, M. Pronine, and P. Richter, Double pendulum and θ -divisor, *J. Nonlinear Sci.* **13**, 157 (2003).
- [20] E. Hackmann and C. Laemmerzahl, Geodesic equation in Schwarzschild-(anti-)de Sitter space-times: Analytical solutions and applications, *Phys. Rev. D* **78**, 024035 (2008).
- [21] E. Hackmann and C. Laemmerzahl, Complete Analytic Solution of the Geodesic Equation in Schwarzschild-(Anti-)de Sitter Spacetimes, *Phys. Rev. Lett.* **100**, 171101 (2008).
- [22] G. Denardo, L. Hively, and R. Ruffini, On the generalized ergosphere of the Kerr-Newman geometry, *Phys. Lett.* **50B**, 270 (1974).
- [23] H. Salazar Ibarguen, A. Garcia, and J. Plebański, Signals in nonlinear electrodynamics invariant under duality rotations, *J. Math. Phys. (N.Y.)* **30**, 2689 (1989).